Хиральная нанофотоника

С. Г. Тиходеев
Физический факультет МГУ им. М.В. Ломоносова
Институт общей физики РАН им. А.М. Прохорова

Величъ, г. Звенигород

Collaboration

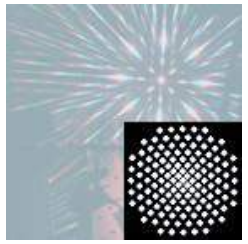

О.А.Дмитриева, Н.В. Валенко
Физический факультет МГУ

С.А.Дьяков, Н.А.Гиппиус, И.М. Фрадкин
Сколковский институт науки и технологии

Thomas Weiss
Universität Graz, Austria & Universität Stuttgart, Germany

А.А.Деменев, Е.В.Филатов, А.А.Максимов, И.И.Тартаковский, В.Д. Кулаковский
Институт физики твердого тела РАН, г. Черноголовка

K. Konishi & M. Kuwata-Gonokami
The University of Tokyo, Tokyo, Japan

THE UNIVERSITY OF TOKYO

C. Schneider
Universität Oldenburg, Germany

S. Höfling
Technische Physik & Wilhelm-Conrad-Röntgen-Research Center for Complex Material Systems, Universität Würzburg, Germany

ПЛАН ЛЕКЦИЙ

1. Введение: хиральность и циркулярно-поляризованный свет, резонансы
2. Фотолюминесценция ахиральных квантовых точек в хиральном диэлектрическим волноводе
3. Как это устройство работает
4. Маршрутизация фотолюминесценции спин-поляризованных квантовых точек из хиральных фотонных структур
5. Лазеры циркулярно-поляризованного излучения на основе хиральных AlGaAs брэгговских микрорезонаторов
6. Мильтистабильности в хиральных микрорезонаторах
7. Метаповерхности с максимальной хиральностью и «закрученный» свет
8. Выводы

ПЛАН ЛЕКЦИИ 2

1. Введение: хиральность и циркулярно-поляризованный свет, резонансы
2. Фотолюминесценция ахиральных квантовых точек в хиральном диэлектрическим волноводе
3. Как это устройство работает
4. Маршрутизация фотолюминесценции спин-поляризованных квантовых точек из хиральных фотонных структур
5. Лазеры циркулярно-поляризованного излучения на основе хиральных AlGaAs брэгговских микрорезонаторов
6. Мильтистабильности в хиральных микрорезонаторах
7. Метаповерхности с максимальной хиральностью и «закрученный» свет
8. Выводы

Handedness-preserving chiral photonic crystal mirror

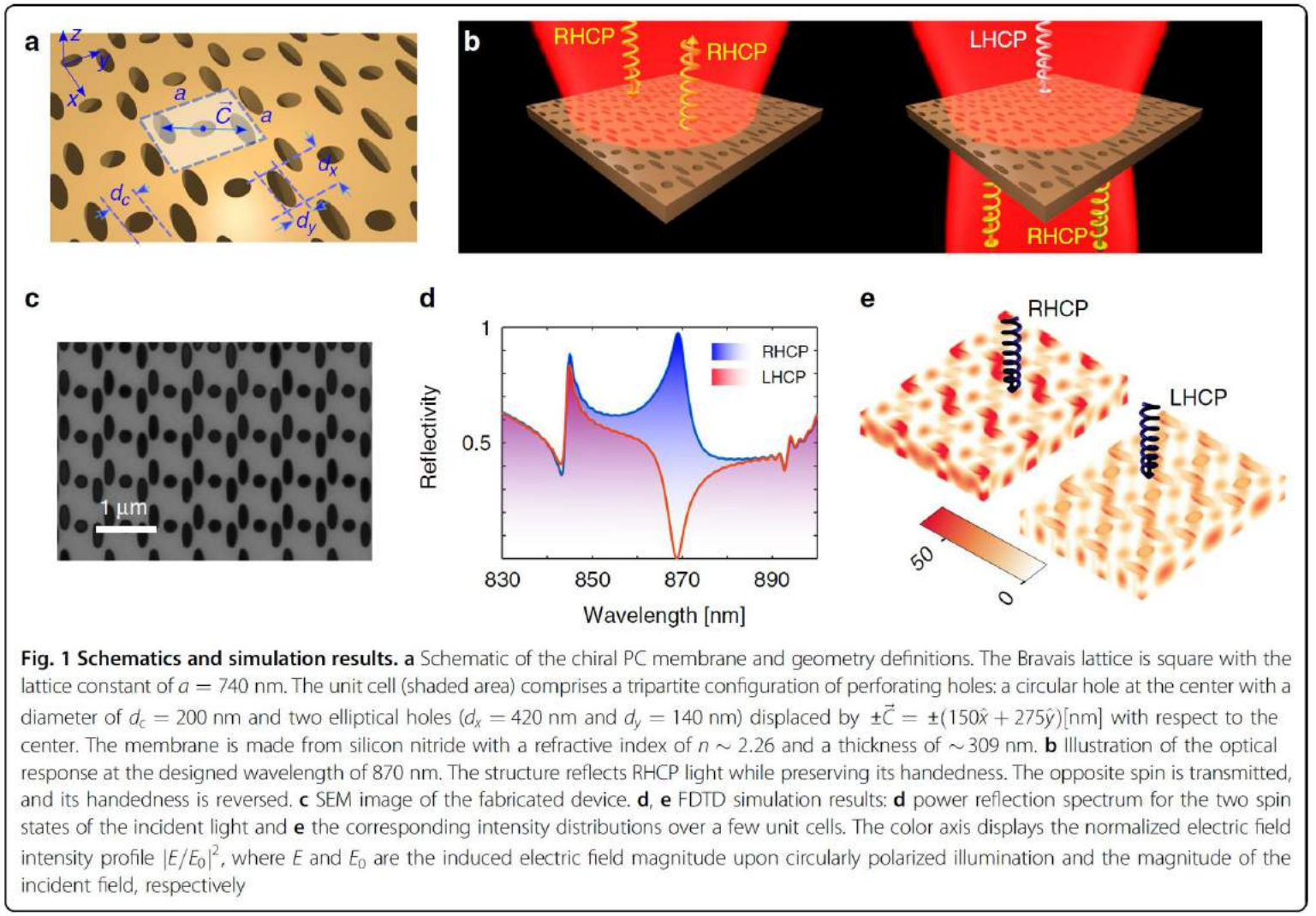

Fig. 1 Schematics and simulation results. a Schematic of the chiral PC membrane and geometry definitions. The Bravais lattice is square with the lattice constant of $a = 740$ nm. The unit cell (shaded area) comprises a tripartite configuration of perforating holes: a circular hole at the center with a diameter of $d_c = 200$ nm and two elliptical holes ($d_x = 420$ nm and $d_y = 140$ nm) displaced by $\pm\vec{C} = \pm(150\hat{x} + 275\hat{y})$[nm] with respect to the center. The membrane is made from silicon nitride with a refractive index of $n \sim 2.26$ and a thickness of ~309 nm. **b** Illustration of the optical response at the designed wavelength of 870 nm. The structure reflects RHCP light while preserving its handedness. The opposite spin is transmitted, and its handedness is reversed. **c** SEM image of the fabricated device. **d**, **e** FDTD simulation results: **d** power reflection spectrum for the two spin states of the incident light and **e** the corresponding intensity distributions over a few unit cells. The color axis displays the normalized electric field intensity profile $|E/E_0|^2$, where E and E_0 are the induced electric field magnitude upon circularly polarized illumination and the magnitude of the incident field, respectively

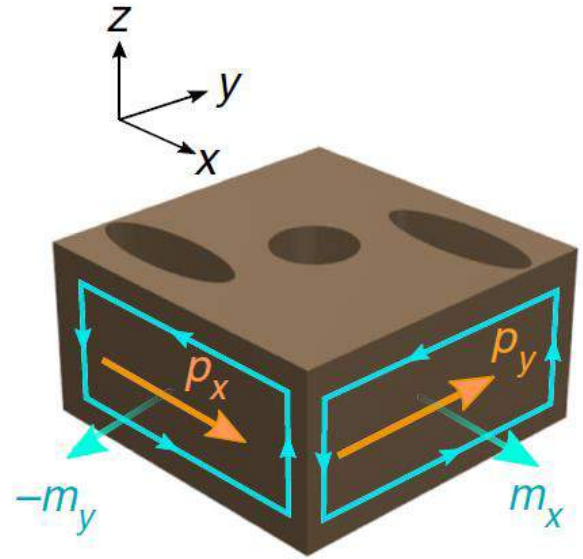

Экспериментальная реализация на слое SiN

Симметрия C2h разрешает конверсию хиральности

Chiral Optical Cavities

ACS Photonics pubs.acs.org/journal/apchd5 Article

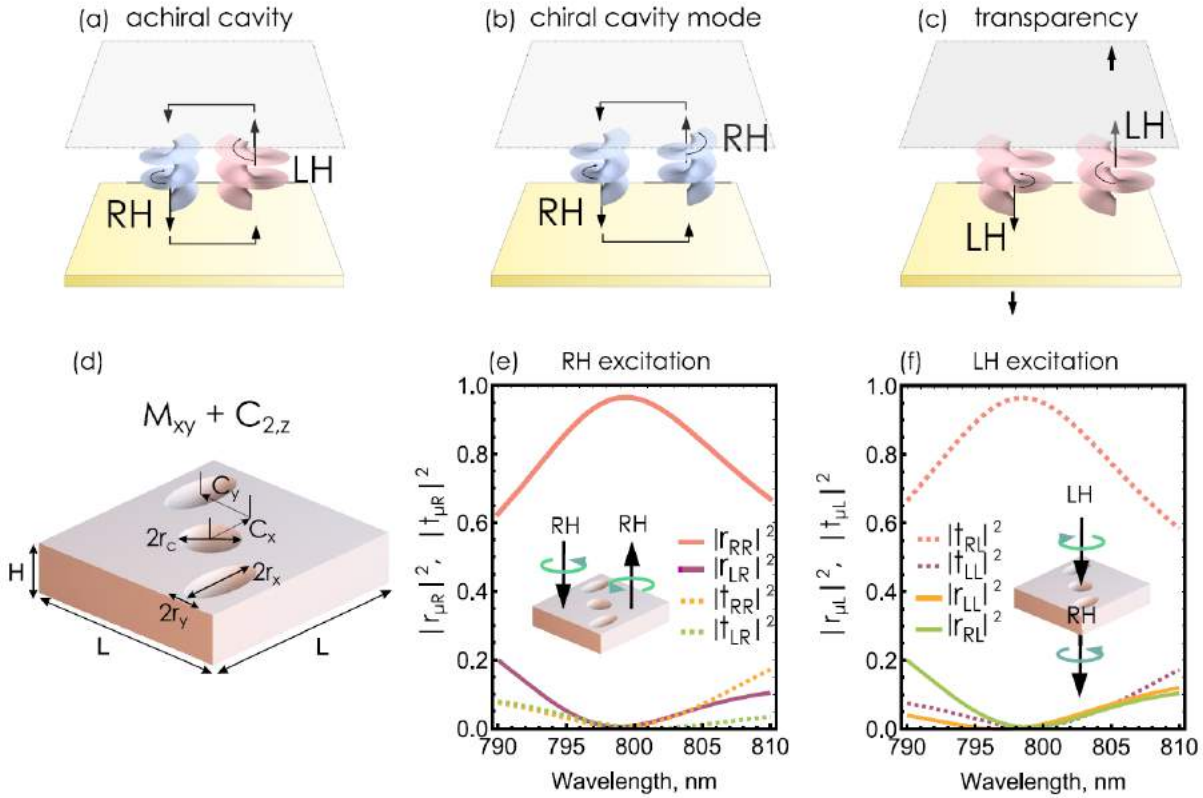

Figure 1. (a–c) Concept of a single-handedness cavity. An ordinary achiral cavity, (a), does not support chiral eigenmodes due to handedness flipping of the standing wave inside the cavity. A single-handedness optical cavity supports a mode of a well-defined handedness, (b), and does not support a mode of the opposite handedness at the same wavelength, (c). (d) The unit cell of the photonic crystal slab mirror featuring handedness-preserving reflection at normal incidence. (e) Reflection and transmission coefficients of the optimized mirror in the circular polarization basis for right-handed incident light exhibiting near-unity reflection with preserved handedness. (f) Reflection and transmission coefficients of the optimized mirror for left-handed incident light exhibiting near-complete transmission accompanied by handedness flipping.

Diamond metasurface with maximum chirality for λ = 10-12 μm

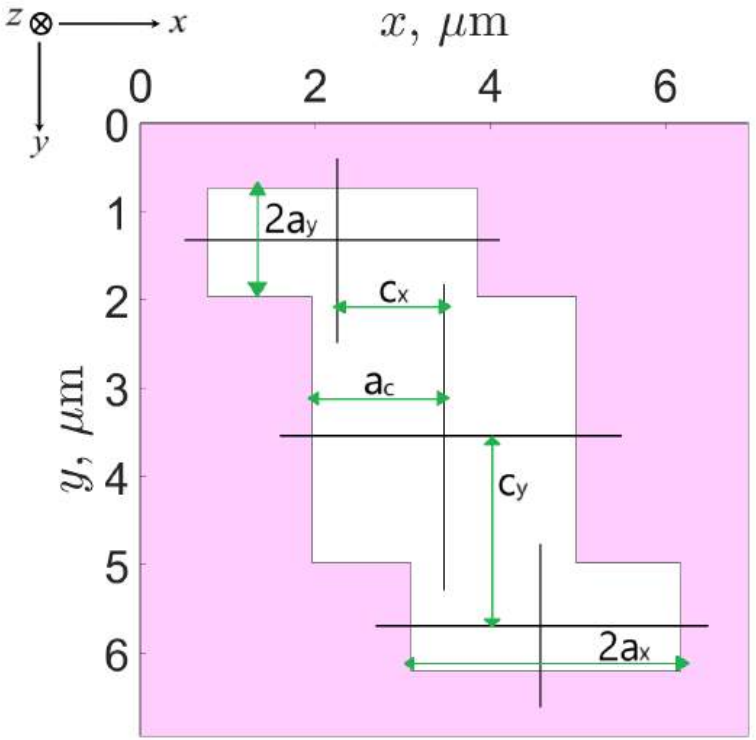

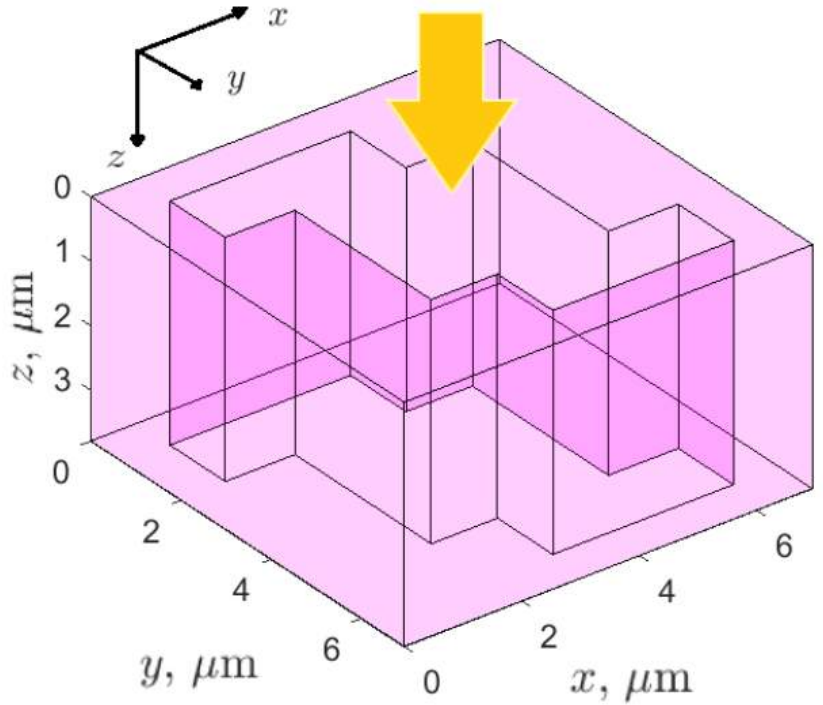

$$CDR = \frac{R_l - R_r}{R_l + R_r}$$

$$R_l = R_{rl} + R_{ll}$$

The cell dimensions are optimized for diamond with dielectric constant ε_D = 5.76 (shown in purple) and achieving maximum chirality at a wavelength of 11 μm and are px = py = 6.95 μm, h = 4 μm .
ac = 1.51 μm, cx = 1.16, cy = 2.12 μm, ax = 1.54 μm, ay = 0.62 μm.

Diamond metasurface with maximum chirality for λ = 10-12 μm

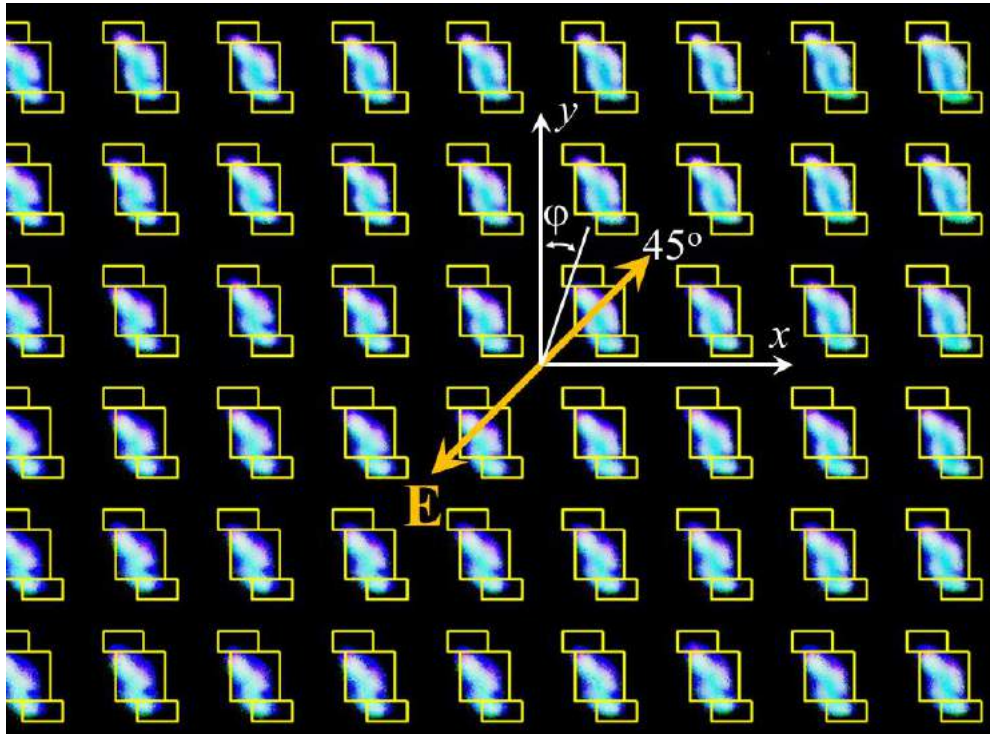

The 1st attempt to manufacture such a membrane by laser ablation
Maxim S. Komlenok et al., in preparation

Optical image (in transmission mode) of a part of the array with the superimposed theoretical mask. The angle of rotation of the polarizer φ is counted from the y-axis as shown in the figure. The yellow double arrow shows the orientation of the electric field of the incident wave at $\varphi = 0$ (along the diagonal between the x and y axes).

Diamond metasurface with maximum chirality for λ = 10-12 μm

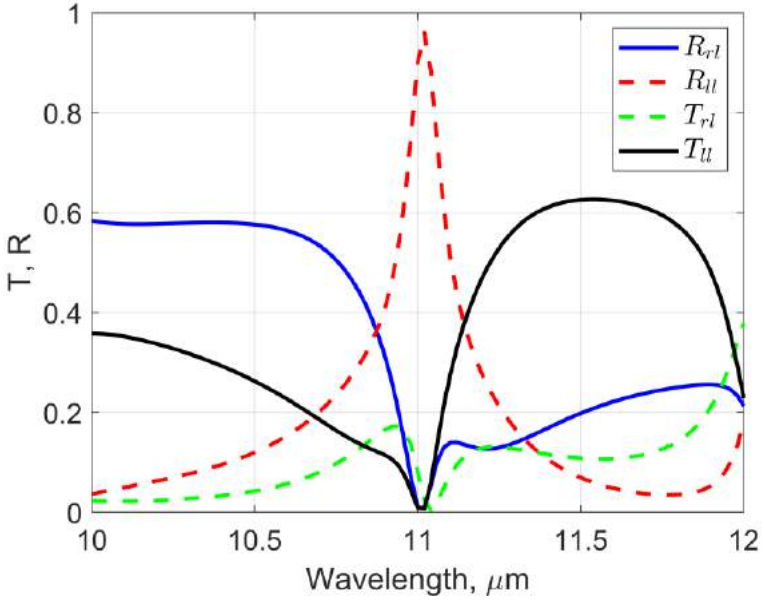

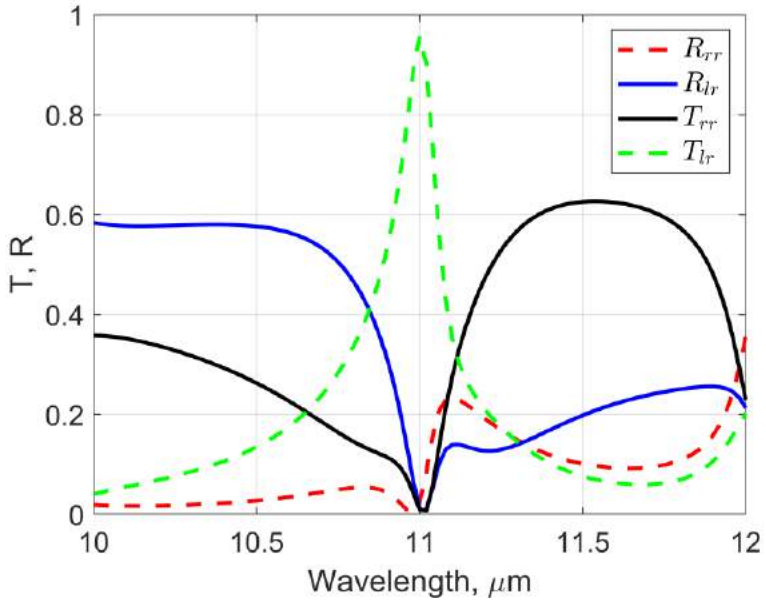

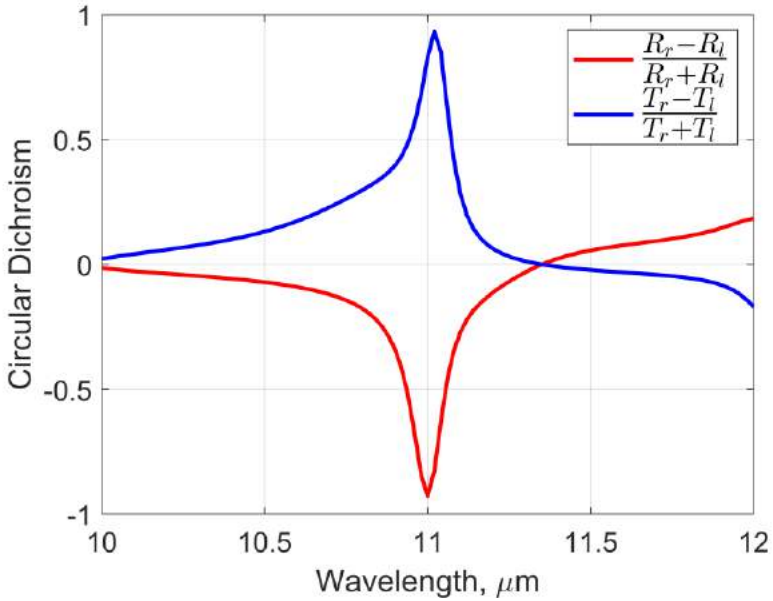

Intensity optical coefficients (real numbers) are related to the corresponding amplitude coefficients (complex numbers)

$$R_{ll} = |r_{ll}|^2, \quad T_{rl} = |t_{rl}|^2, \quad \dots.$$

Electrodynamic reciprocity leads to:

$$r_{lr} = r_{rl}, \quad t_{rr} = t_{ll}$$

$$R_{lr} = R_{rl}, \quad T_{rr} = T_{ll}$$

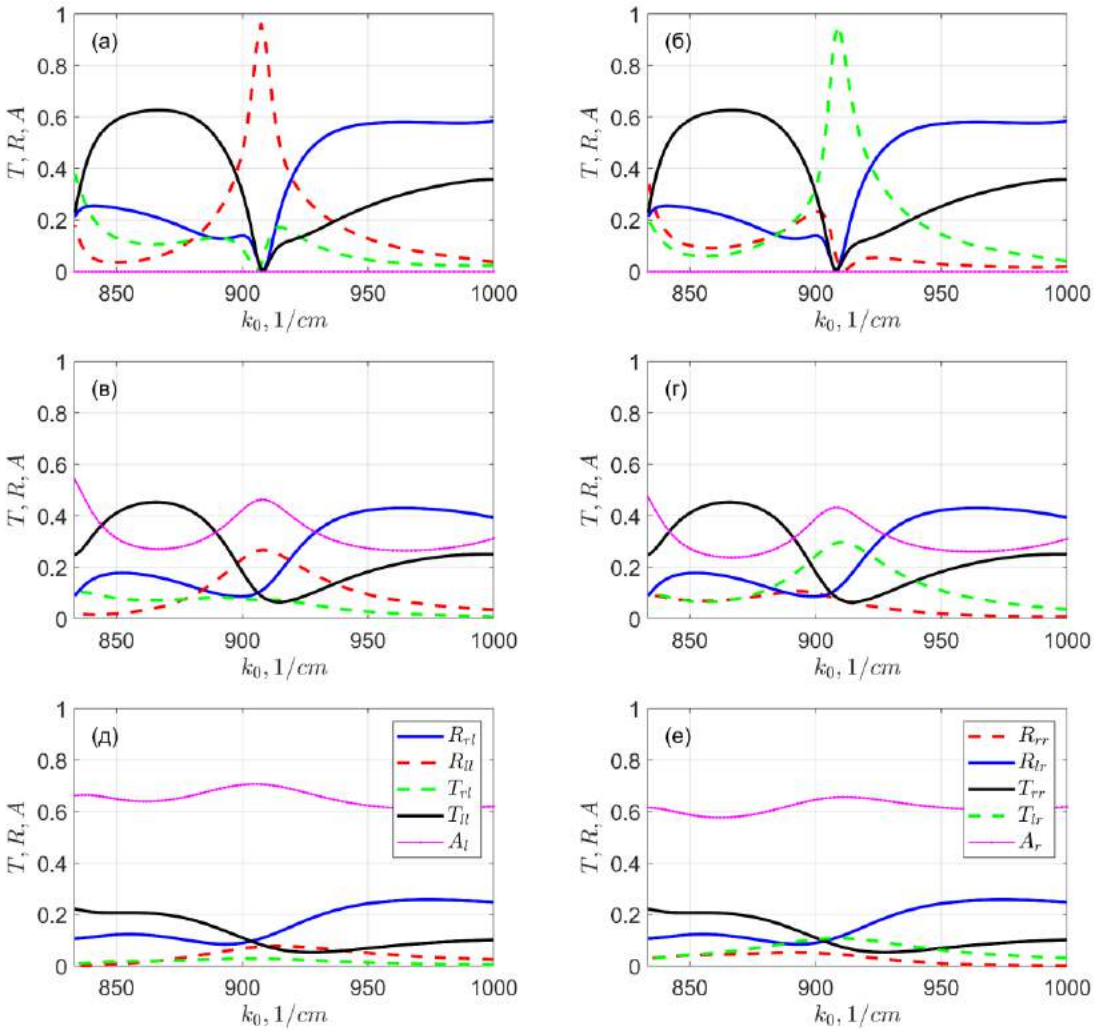

Наличие потерь существенно уменьшает эффект

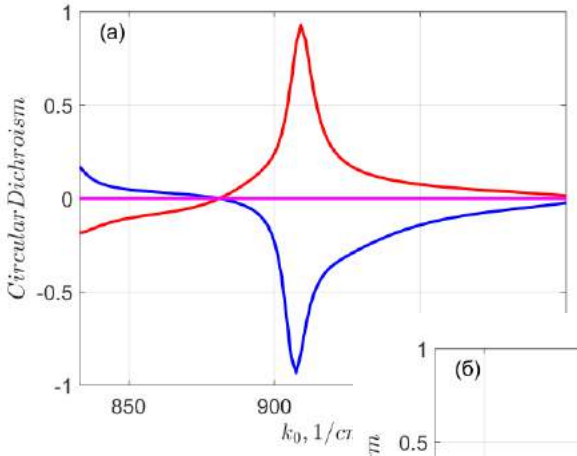

A=5

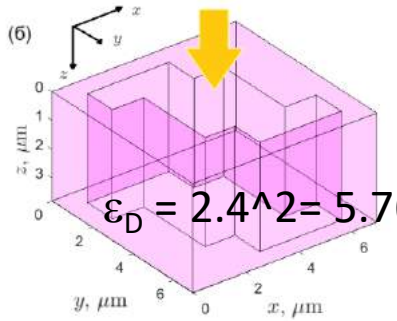

$\varepsilon_D = 2.4^2 = 5.76$

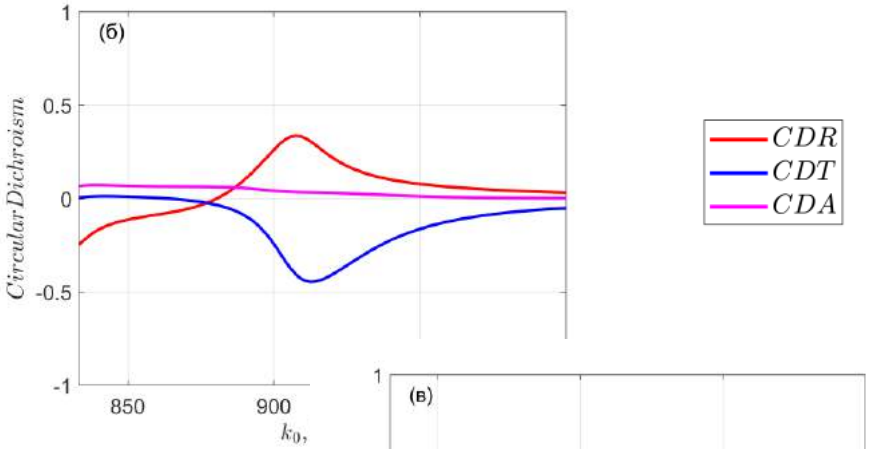

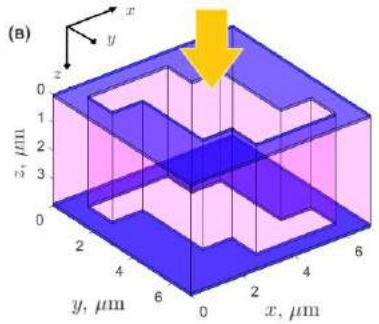

$\varepsilon_A = 5.76 + 1i*A;$

A=50

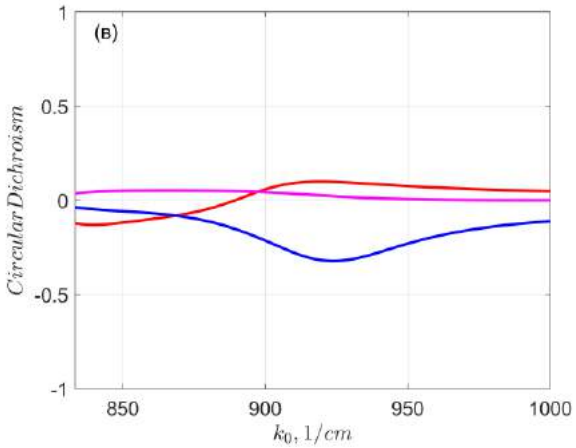

ADVANCED SCIENCE NEWS
www.advancedsciencenews.com

ADVANCED OPTICAL MATERIALS
www.advopticalmat.de

Chiral Light in Twisted Fabry–Pérot Cavities

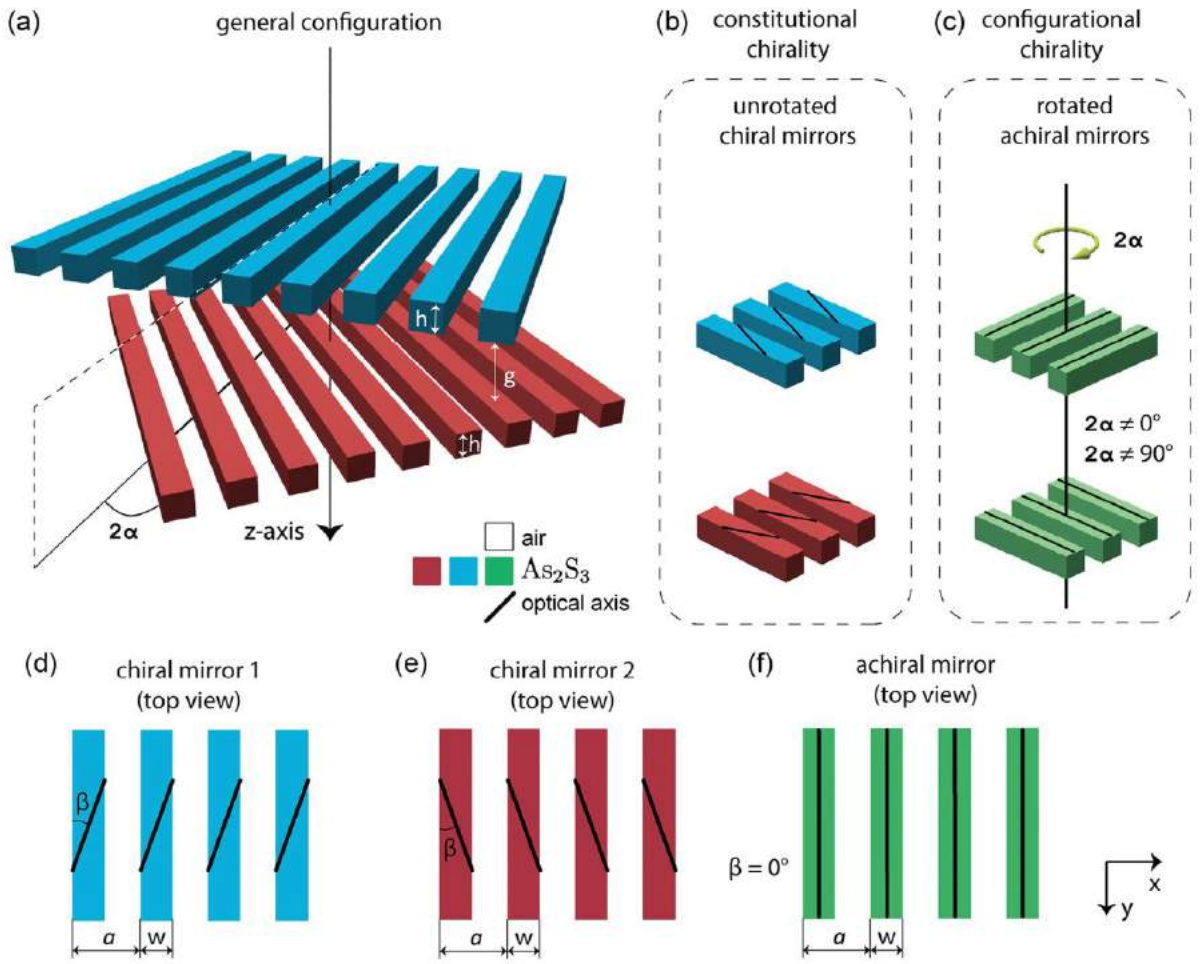

Figure 1. a) The most general configuration of a chiral resonator with twisted one-dimensional gratings. b) Chiral resonators formed by chiral and non-chiral mirrors. c) A top view of the unrotated chiral and non-chiral mirrors. In (a–f) color represents the orientation of optical axis.

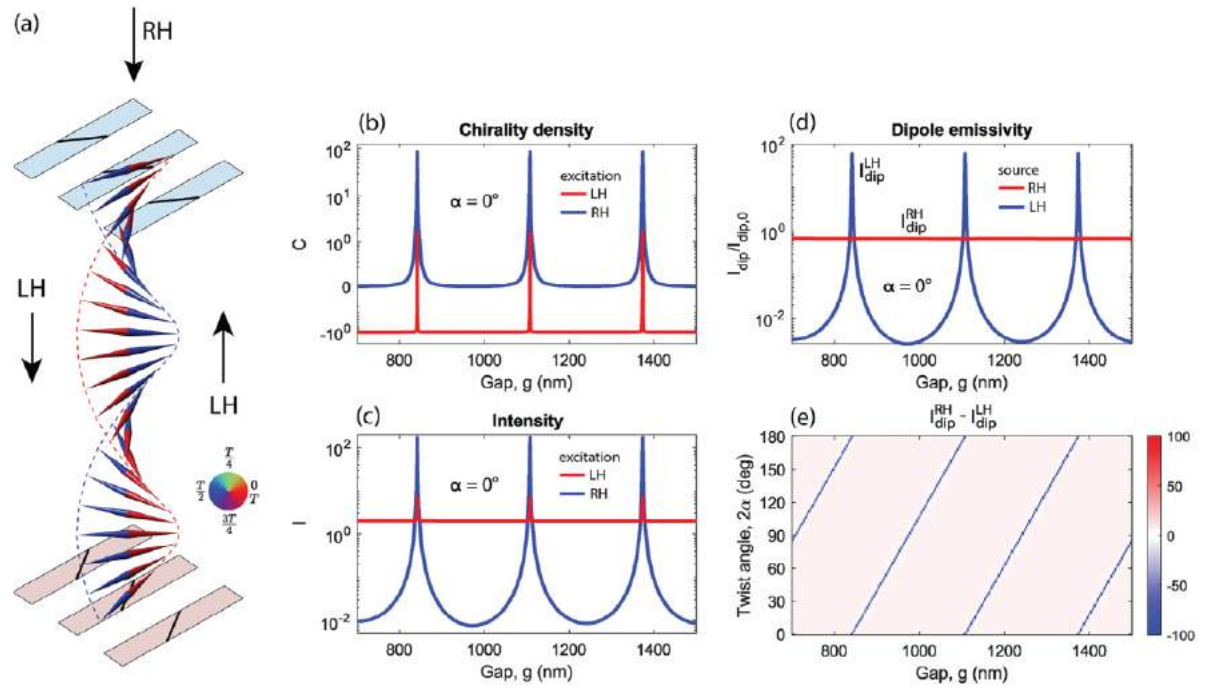

Figure 3. a) Sketch view of a chiral resonator supporting LH Fabry–Pérot modes. The cones represent electric vectors of the incident wave settled in the gap between the mirrors, with phases specified by the circular colorbar. The field distribution is calculated for the gap size $g \approx 575$ nm and the twist angle $2\alpha = 0°$. The gap-size dependence of b) the time-average normalized chirality density and c) normalized intensity in the middle of the cavity. d) The gap-size dependence of the emissivity of RH and LH dipole sources placed in the middle of the cavity. e) The gap-size and twist-angle dependence of a difference between RH and LH dipole emissivities.

ADVANCED SCIENCE NEWS
www.advancedsciencenews.com

ADVANCED OPTICAL MATERIALS
www.advopticalmat.de

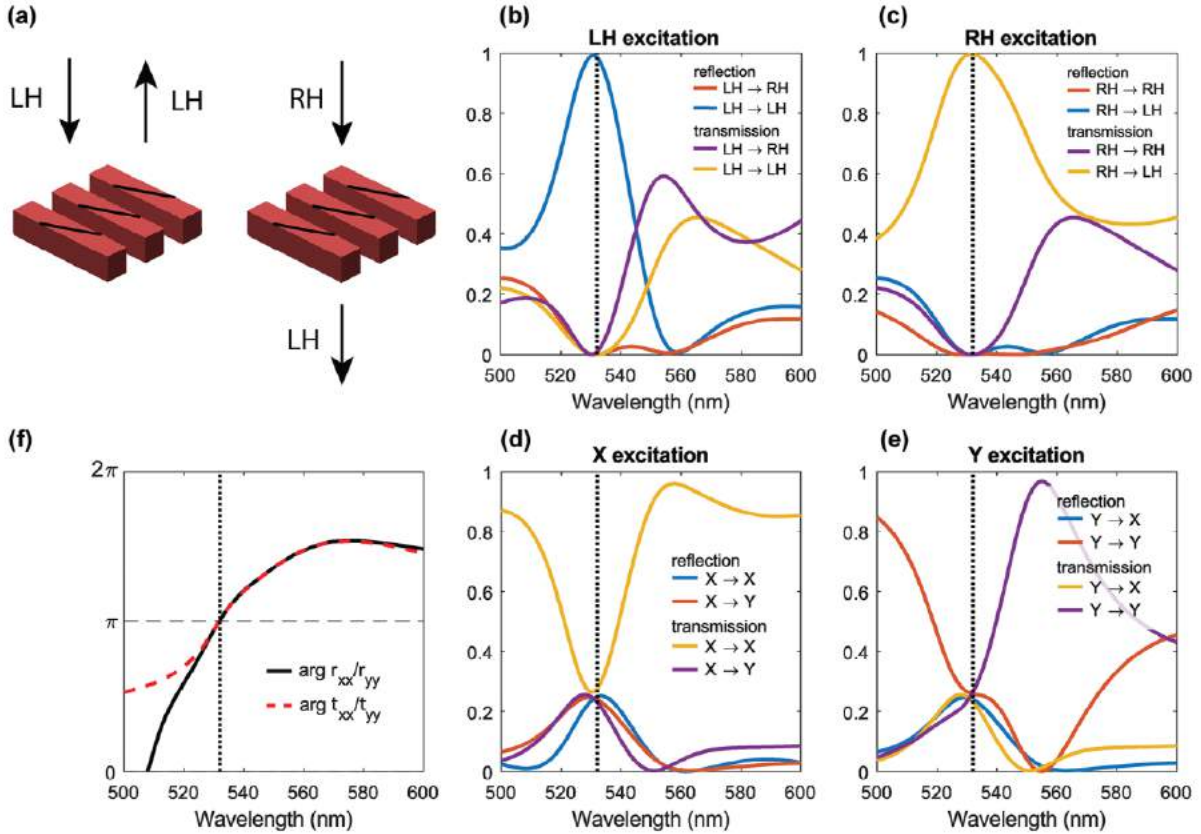

Figure 2. a) Schematic view of the lower chiral grating, designed to reflect the LH light and transmit the RH light. b,c) The cross-polarized reflection and transmission coefficients of the chiral grating for RH and LH incident light. d,e) The cross-polarized reflection and transmission coefficients of the chiral grating upon *X*- and *Y*-polarized incident light. f) The phase difference between the r_{xx} and r_{yy} coefficients (black solid line) and between the t_{xx} and t_{yy} coefficients (red dashed line).

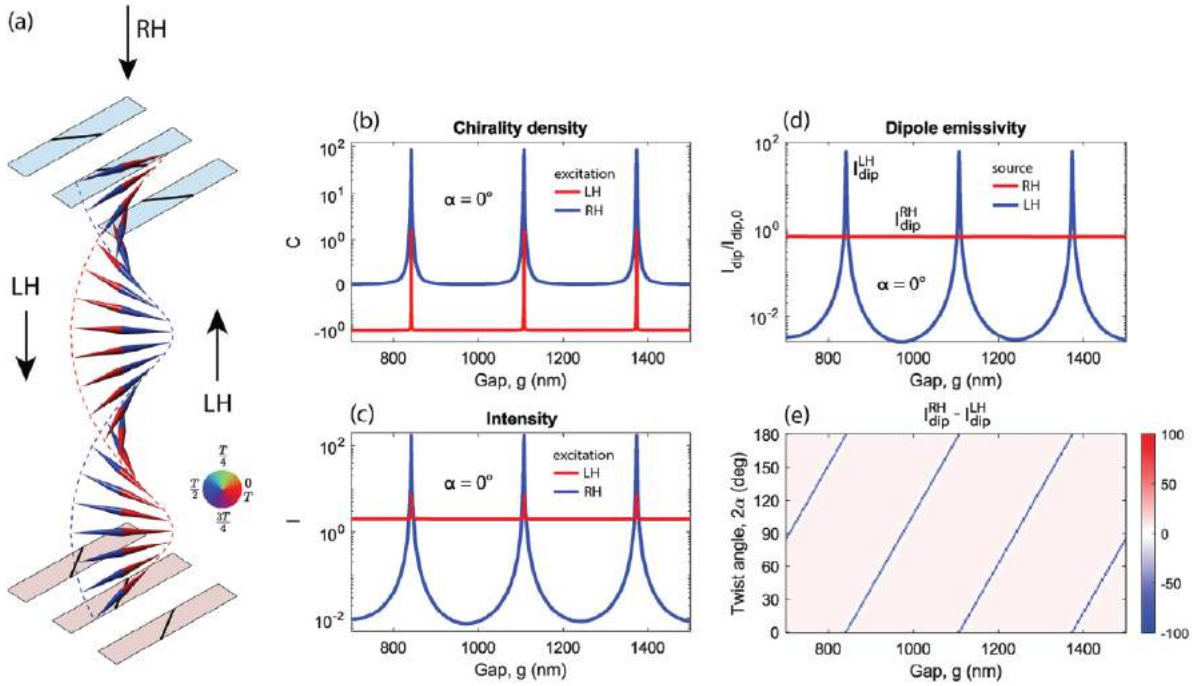

Figure 3. a) Sketch view of a chiral resonator supporting LH Fabry–Pérot modes. The cones represent electric vectors of the incident wave settled in the gap between the mirrors, with phases specified by the circular colorbar. The field distribution is calculated for the gap size $g \approx 575$ nm and the twist angle $2\alpha = 0°$. The gap-size dependence of b) the time-average normalized chirality density and c) normalized intensity in the middle of the cavity. d) The gap-size dependence of the emissivity of RH and LH dipole sources placed in the middle of the cavity. e) The gap-size and twist-angle dependence of a difference between RH and LH dipole emissivities.

Chiral Polaritonics

ABSTRACT: Preferential selection of a given enantiomer over its chiral counterpart has become increasingly relevant in the advent of the next era of medical drug design. In parallel, cavity quantum electrodynamics has grown into a solid framework to control energy transfer and chemical reactivity, the latter requiring strong coupling. In this work, we derive an analytical solution to a system of many chiral emitters interacting with a chiral cavity similar to the widely used Tavis−Cummings and Hopfield models of quantum optics. We are able to estimate the discriminating strength of chiral polaritonics, discuss possible future development directions and exciting applications such as elucidating homochirality, and deliver much needed intuition to foster the newly flourishing field of chiral polaritonics.

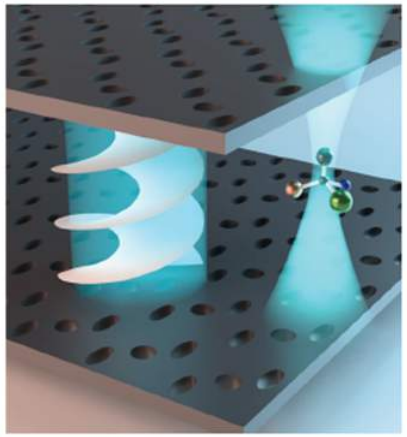

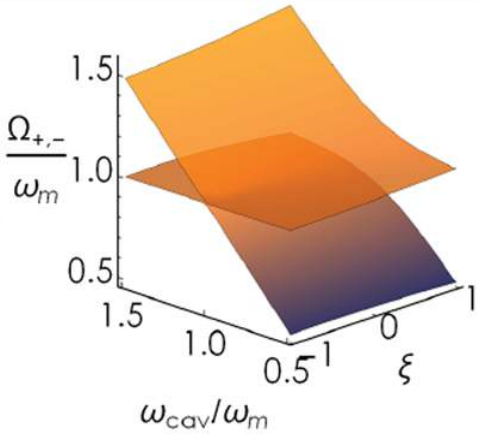

Advent of the next era of medical drug design

Грядет новая эра в разработке медицинских препаратов

Выводы

- Хиральные фотонные структуры – компактные источники циркулярно-поляризованной фотолюминесценции как в спонтанном, так и лазерном режиме.
- Хиральные метаповерхности для маршрутизации фотолюминесценции по спину излучателя
- Хиральные метаповерхности с максимальной хиральностью для создания микрорезонаторов закрученного света.
- Потенциальные области применения: спектроскопия, сенсорика, включая био-сенсорику, медицина и фармакологическая промышленность, спинтроника.

Работа выполнена при поддержке РНФ (проект № 22-12-00351).

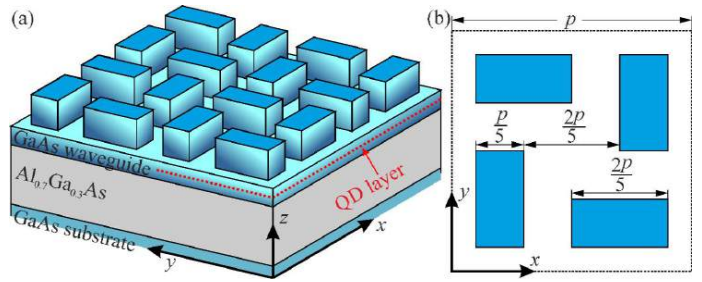

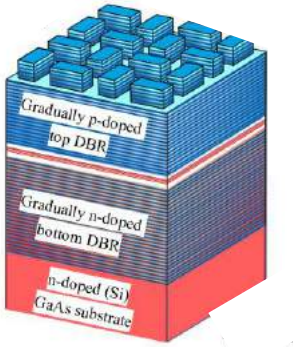

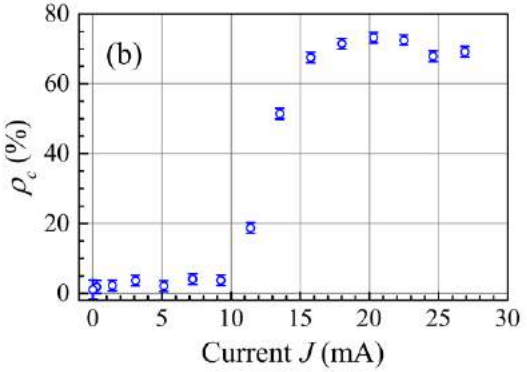

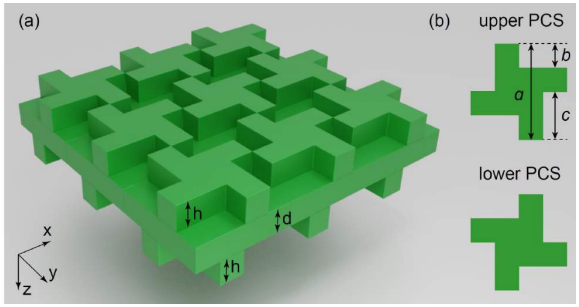

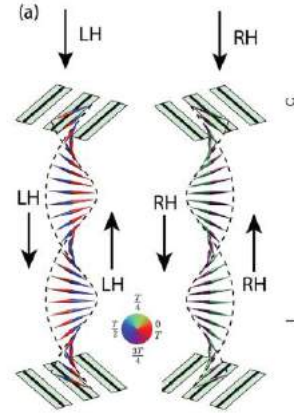

СПАСИБО ЗА ВНИМАНИЕ!